Dalton Transactions

Cite this: *Dalton Trans.*, 2012, **41**, 11788

www.rsc.org/dalton

PAPER

# Spectroscopic and magnetic properties of an iodo $Co^{I}$ tripodal phosphine complex†

**Michael J. Rose, Donatela E. Bellone, Angel J. Di Bilio and Harry B. Gray***

***Received 7th June 2012, Accepted 31st July 2012***
**DOI: 10.1039/c2dt31229h**



Reaction of the tripodal phosphine ligand 1,1,1-tris((diphenylphosphino)phenyl)ethane (PhP3) with $CoI_2$ spontaneously generates a one-electron reduced complex, [(PhP3)$Co^{I}$(I)] (**1**). The crystal structure of **1** reveals a distorted tetrahedral environment, with an apical Co–I bond distance of ~2.52 Å. $Co^{II/I}$ redox occurs at an unusually high potential (+0.38 V *vs.* SCE). The electronic absorption spectrum of **1** exhibits an MLCT peak at 320 nm ($\varepsilon$ = 8790 $M^{-1}$ $cm^{-1}$) and a d–d feature at 850 nm ($\varepsilon$ = 840 $M^{-1}$ $cm^{-1}$). Two more d–d bands are observed in the NIR region, 8650 ($\varepsilon$ = 450) and 7950 $cm^{-1}$ ($\varepsilon$ = 430 $M^{-1}$ $cm^{-1}$). Temperature dependent magnetic measurements (SQUID) on **1** (solid state, 20–300 K) give $\mu_{eff}$ = 2.99(6) $\mu_B$, consistent with an $S$ = 1 ground state. Magnetic susceptibilities below 20 K are consistent with a zero field splitting (zfs) $|D|$ = 8 $cm^{-1}$. DFT calculations also support a spin-triplet ground state for **1**, as optimized (6-31G*/PW91) geometries ($S$ = 1) closely match the X-ray structure. EPR measurements performed in parallel mode (X-band; 0–15 000 G, 15 K) on polycrystalline **1** or frozen solutions of **1** (THF/toluene) exhibit a feature at $g \approx 4$ that arises from a ($\Delta m$ = 2) transition within the $M_S$ = <+1,−1> manifold. Below 10 K, the EPR signal decreases significantly, consistent with a solution zfs parameter ($|D| \approx 8$ $cm^{-1}$) similar to that obtained from SQUID measurements. Our work provides an EPR signature for high-spin $Co^{I}$ in trigonal ligation.

## Introduction

The isolation of low-valent transition metal complexes ($M^{I/0}$) has been pursued to probe intermediates in catalytic reaction pathways, and to establish new electronic descriptions of metals in low oxidation states.[1–5] Cobalt phosphines are of interest due to their use as catalysts in hydroformylation reactions,[6] Reformatski transformations,[7] Diers–Alder type cycloadditions,[8] olefin insertions[9] and hydroarylation methodology.[10,11] In such transformations, *in situ* activation of $Co^{II}$ starting materials with reducing agents such as sodium amalgam, magnesium turnings or zinc powder is required to form the active catalyst. Some of these active catalyst species have been structurally characterized, as in the case of an ethylene-bound $Co^{I}$ triphosphine complex.[9b] However, in most cases, the structural, magnetic and spectroscopic properties of the relevant $Co^{I}$ intermediates remain undefined, partially due to the difficulty of detecting and characterizing paramagnetic $Co^{I}$ species by traditional techniques (*e.g.* EPR and NMR).

Several pseudo-tetrahedral $Co^{I}$ complexes of general formula [$(R_3P)_3Co^{I}(X)$] (where R = Me, Ph; X = Cl, Br, I)[12–15] have been prepared *via* reduction of the corresponding $Co^{II}$ species. In early work, Sacconi and Midollini reported similar preparations for the analogous $Co^{I}$–X phosphine species derived from tetradentate tripods as in the case of [(NP3)Co(X)][16] or [(PP3)-Co(X)].[17] In contrast, employing tridentate, tripodal phosphine 1,1,1-tris((diphenylphosphino)ethane (MeP3) in conjunction with $CoI_2$ under refluxing conditions led to spontaneous reduction of $Co^{II}$ to $Co^{I}$;[18] this complex was not structurally characterized. By comparison, preparation of the corresponding chloro or bromo species required reduction with $NaBH_4$.[18] In subsequent work, Schober and coworkers prepared a series of $Co^{II}$ complexes derived from MeP3, including the structurally characterized $Co^{I}$ species [(MeP3)$Co^{I}$(Cl)] (*via* reduction of [(MeP3)$Co^{II}(Cl)_2$] with Na/Hg).[19a] In this case, a very strong reductant was required, owing to the negative $Co^{II/I}$ reduction potential (−850 mV *vs.* SCE) in THF solution.[19a] All in all, there are many reported $Co^{II}$ [18,19a,b] and $Co^{I}$ [18,19a,c,d] complexes derived from MeP3.

Peters and coworkers have extensively explored cobalt complexes coordinated by an anionic, tripodal ligand $PhB(CH_2PR_2)_3$ (or PhBP3)[20] or $Si(CH_2PR_2)_3$ (or SiP3).[21] In a related example of cobalt–phosphine–iodide redox chemistry, these investigators reported spontaneous reduction of [(PhBP3)$Co^{II}$(I)] in the presence of excess CO to generate [(PhBP3)$Co^{I}(CO)_2$],[22] presumably along with 1/2 equivalent of $I_2$; interestingly, the corresponding chloro species did not auto-reduce to $Co^{I}$.[22] In more recent work, Thomas and coworkers observed spontaneous formation of $Co^{I}$ in a heterobimetallic Zr–Co system upon metallation of

*Beckman Institute, California Institute of Technology, Pasadena, CA 91125, USA. E-mail: hbgray@caltech.edu*

†CCDC 811870. For crystallographic data in CIF or other electronic format see DOI: 10.1039/c2dt31229h

[$(R_2PNR')_3Zr(Cl)$] (where R = Ph, $^i$Pr; R′ = $^i$Pr, Mes) with $CoI_2$.[23] The authors suggested that $I^-$ was the likely reducing agent, with $I_2$ generated as byproduct; reaction of $CoCl_2$ under the same conditions did not generate the $Co^I$ species. Notably, after two-electron reduction, the Zr–Co complex activates carbon dioxide at the Co center.[23]

In keeping with triphosphine precedents, we have employed an MeP3 analogue with a substituted phenyl appendage, namely 1,1,1-tris((diphenylphosphino)phenyl)-ethane (PhP3).[24–26] We initially selected this ligand on the basis of its suitability for functionalization at the *para* position for surface/photoelectrode attachment, an ongoing aim in our laboratory. Although PhP3 is structurally analogous to MeP3, only one complex has been reported previously, namely, [(PhP3)Ru(Cl)$_2$],[26] which was not structurally characterized.

Spectroscopic characterization of paramagnetic integer-spin systems such as high-spin $Co^I$, $Fe^{II}$, and $Ni^{II}$ has typically relied on magnetic circular dichroism (MCD)[27–29] or far-infrared magnetic spectrosopy.[30] Telser and coworkers have pioneered high-field electron paramagnetic resonance (HFEPR) as a way to probe integer spin systems, including those in the $d^8$ class ($Ni^{II}$, $Co^I$).[31,32] While this is a powerful technique that provides an unambiguous spectroscopic signature, it requires access to advanced instrumentation that is not present in conventional inorganic laboratories. Within the last decade, several groups[33–38] have utilized parallel mode EPR at conventional magnetic field strengths to probe $d^2$ ($Mn^V$), $d^4$ ($Fe^{IV}$, $Mn^{III}$) and other integer spin systems in small molecule or protein environments (see the EPR section for further references and details). In this work, we report the parallel mode EPR signature of [(PhP3)$Co^I$(I)] at conventional magnetic fields (0–6000 G, X-band) as an example of EPR detection of a non-Kramers $d^8$ system.

## Experimental

### Reagents and general procedures

Phenylacetaldehyde, paraformaldehyde, $^t$BuOK and cobalt(II) iodide were obtained from Sigma-Aldrich. Thionyl chloride from Alfa-Aesar was distilled before use. The ligand PhP3 was synthesized according to published procedures,[24–26] and metalations were performed under $N_2$ atmosphere at room temperature. Pyridine and $CH_2Cl_2$ from J.T. Baker were used without further purification, while other solvents (MeCN, THF, $Et_2O$ and toluene) were from a solvent purification system described previously.[39] Deuterated solvents from Cambridge Isotopes were used as received.

### Synthetic procedure. [(PhP3)Co(I)] (1)

Anhydrous cobalt iodide (23 mg, 0.073 mmol) was dissolved in 5 mL THF and added dropwise to a stirred solution of PhP3 (50 mg, 0.073 mmol) in 10 mL THF under $N_2$ atmosphere to generate a greenish-brown solution. After stirring for 12 h at room temperature, the orange solution was concentrated *in vacuo* to 5 mL. Storage of the solution at −20 °C for several days afforded an orange microcrystalline material. Yield: 60 mg (54%). X-ray quality crystals were obtained by vapor diffusion of $Et_2O$ into a concentrated THF solution of **1** at room temperature over the course of several days. UV/vis/NIR, $\lambda$ in nm ($\varepsilon$ in $M^{-1}$ $cm^{-1}$): 270 (8950), 325 (8800), 870 (230), 1150 (450), 1260 sh (430). Magnetic susceptibility (solid state): $\mu_{eff}$ = 2.99(6) $\mu_B$, 20–300 K. Anal. calcd for $C_{46}H_{44}CoIP_3$, C 63.15, H 5.12; found C 64.83, H 5.73.

### Physical measurements. X-ray crystallography

Crystals were mounted on a glass fiber using Paratone oil then placed on the diffractometer under a stream of $N_2$ at 100 K. Refinement of $F^2$ against all reflections: the weighted *R*-factor (w*R*) and goodness of fit (*S*) were based on $F^2$, conventional *R*-factors (*R*) were based on *F*, with *F* set to zero for negative $F^2$. The threshold expression $F^2 > 2\sigma(F^2)$ was used only for calculating *R*-factors(gt) etc; it was not relevant to the choice of reflections for refinement. Diffraction intensity data were collected on a Bruker Kappa APEX II diffractometer equipped with a MoKα X-ray source; data were collected using APEX2 v2009.7-0; the data reduction program SAINT-plus v7.66A was used. Details of the data collection and refinement are given in Tables 1 and 2.

### Magnetic susceptibility measurements

Temperature dependent magnetic susceptibilities of [(PhP3)-Co(I)] (**1**) were recorded using a Quantum Designs SQUID magnetometer controlled by MPMSR2 software. Data points were acquired from 4 to 300 K at 5000 and 50 000 G, and the diamagnetic contributions were corrected using Pascal's constants.[40] The output was converted to effective magnetic moment ($\mu_{eff}$) and plotted (as $\mu_B$) *versus* temperature (K).

**Table 1** Crystal data and refinement parameters for **1**

| | **1**·THF·$Et_2O$ |
|---|---|
| Empirical formula | $C_{46}H_{41}IP_3Co{\cdot}C_4H_8O{\cdot}C_4H_{10}O$ |
| Fw | 945.19 |
| Color | Orange |
| Habit | Block |
| Size (mm) | 0.20 × 0.16 × 0.16 |
| *T* (*K*) | 100(2) |
| Wavelength (Å) | 0.71073 |
| Lattice system | Orthorhombic |
| Space group | $P2_12_12_1$ |
| *a* (Å) | 19.1082(7) |
| *b* (Å) | 21.2045(9) |
| *c* (Å) | 21.4894(9) |
| *α* (°) | 90 |
| *β* (°) | 90 |
| *γ* (°) | 90 |
| *V* (Å$^3$) | 8707.1(6) |
| Z | 8 |
| $d_{calc}$ (g $cm^{-3}$) | 1.442 |
| $\mu$ ($mm^{-1}$) | 1.250 |
| GOF on $F^2$ | 1.689 |
| Final *R* indices | $R_1$ = 0.0558 |
| [$I > 2\sigma(I)$] | w$R_2$ = 0.0625 |
| *R* indices | $R_1$ = 0.00813 |
| All data | w$R_2$ = 0.0642 |

**Table 2** Selected bond distances (Å) and angles (°) from the X-ray structure of **1**; DFT optimized geometries using the indicated functionals and basis sets[a]

| | **1** | **1′** | **1**$^{avg}$ | **1** (DFT) PW91 6-31G* | **1** (DFT) PW91 TZV | **1** (DFT) B3PW91 6-31G* | **1** (DFT) B3PW91 TZV |
|---|---|---|---|---|---|---|---|
| Co–P1 | 2.1953(14) | 2.2239(12) | 2.215(12) | 2.188 | 2.286[c] | 2.237[b] | 2.441[c] |
| Co–P2 | 2.2052(14) | 2.2259(13) | — | 2.192 | 2.287[c] | 2.242[b] | 2.431[c] |
| Co–P3 | 2.2219(14) | 2.2160(13) | — | 2.192 | 2.285[c] | 2.242[b] | 2.322[c] |
| Co–I | 2.5304(6) | 2.5192(6) | 2.525(8) | 2.536 | 2.530 | 2.574[b] | 2.578[b] |
| P1–Co–I | 122.66(4) | 125.59(4) | 124.1(2) | 122.6 | 124.7 | 123.5 | 123.2 |
| P2–Co–I | 122.85(4) | 122.06(3) | — | 122.9 | 124.5 | 123.8 | 124.8 |
| P3–Co–I | 126.16(4) | 125.04(4) | — | 122.3 | 124.1 | 123.5 | 127.6[b] |
| P1–Co–P2 | 91.39(6) | 91.73(5) | 91.7(7) | 94.45[b] | 91.75 | 92.60 | 88.82[b] |
| P2–Co–P3 | 92.27(5) | 92.28(5) | — | 92.68 | 91.54 | 91.33 | 90.46 |
| P3–Co–P1 | 92.01(6) | 90.36(5) | — | 93.99[b] | 90.26 | 93.03 | 90.75 |

[a] (Note: in all cases, the basis set for the I atom was 6-311G*). [b] Denotes > ~0.2 Å (or >~2°) difference between DFT optimized and X-ray parameters. [c] Denotes > ~0.5 Å difference between DFT optimized and X-ray parameters.

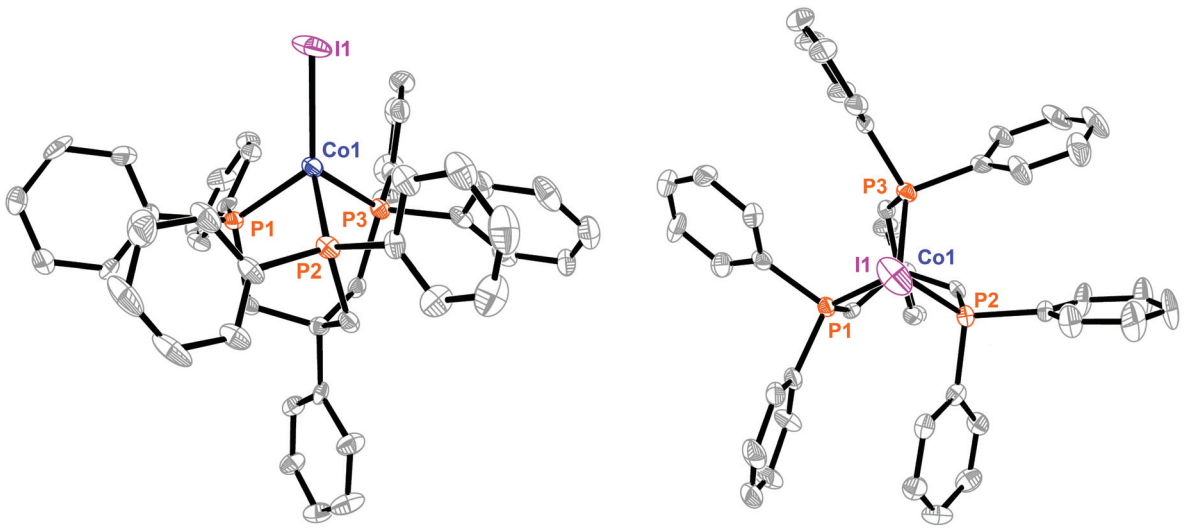


**Fig. 1** Side (left) and top (right) views of ORTEP diagrams (50% thermal ellipsoids) of one of the two [(PhP3)Co(I)] (**1**) molecules in the asymmetric unit.

### Spectroscopy

$^{1}$H and $^{31}$P NMR spectra (in ligand synthesis) were recorded on a Varian Mercury 300 MHz spectrometer and chemical shifts were referenced to TMS and $H_3PO_4$, respectively. UV/vis spectra were obtained using a Cary 50 spectrophotometer at 298 K; vis/NIR spectra were recorded in d$^{8}$-THF (Cambridge Isotopes) on a Cary 5000 UV/vis/NIR instrument. EPR spectra were recorded using a Bruker EMX Biospin spectrometer with a Gunn diode microwave source (X-band). Parallel mode (9.40 GHz) and perpendicular mode (9.60 GHz) spectra were obtained using an ER-4116DM dual mode resonance cavity from Bruker.

### DFT calculations

Geometry optimization and orbital calculations were performed using the PW91[41] and B3PW91[42] functionals in conjunction with 6-31G* and TZV basis sets (note: iodine was calculated using the 6-311G* basis set in all cases). DFT calculations were performed using the Firefly software package.[43] Orbitals were visualized using MacMolPlt,[44] and spin density plots were generated using gOpenMol.[45]

## Results and discussion

### Synthesis and X-ray structure

The ligand PhP3 was synthesized in three steps according to published procedures.[24–26] Reaction of PhP3 with anhydrous $CoI_2$ in THF under inert ($N_2$) atmosphere at room temperature over 12 h generated an orange colored solution. Concentration of the solution followed by addition of $Et_2O$ afforded orange microcrystalline material in good yield (60%). Large orange blocks of X-ray quality were obtained by vapor diffusion of $Et_2O$ into a THF solution of the complex. The structure of the resulting product [(PhP3)Co(I)]·THF·$Et_2O$ (**1**·THF·$Et_2O$ in $P2_12_12_1$) is shown in Fig. 1. The structure reveals a Co center chelated in

 

pseudo-tetrahedral geometry to the three phosphine donors of PhP3 and one coordinated iodide. The Co–P bond lengths of 2.2239(12), 2.2259(13) and 2.2160(13) Å are nearly identical with the Co–P distances (avg = 2.229(30) Å) found in a related $Co^{II}$ complex, $[(MeP3)Co^{II}(Cl)_2]$.[19] The average Co–P distance (2.222(4) Å) also is similar to that in $[(MeP3)Co^{I}(Cl)]$ (avg Co–P = 2.242(3) Å).[19] The P–Co–I bond angles in **1** are similar (125.59(4), 122.06(3) and 125.04(4)°) and indicative of pseudo-*C*3 symmetry; there is, however, no crystallographic symmetry within the complex itself. The structure of **1** revealed only a single $I^-$ ligand bound to the cobalt center, and no counterion ($I^-$ or other) is present in the lattice. The Co–I distance of 2.5192(6) Å is shorter than that in $[(PMe_3)_3Co(I)]$ (Co–I = 2.549 Å),[14] likely due to the stronger σ-donor strength of the $PMe_3$ ligands. However, the Co–I bond in **1** is longer than that of $[(NP3)Co(I)]^+$ (Co–I = 2.466(2) Å),[46] which contains a $Co^{II}$ center bound to an uncharged trigonal phosphine.

There is precedence for the spontaneous formation of $Co^{I}$ in presence of iodide, as Sacconi and coworkers obtained [(MeP3)-Co(I)] from $CoI_2$ and MeP3 under refluxing conditions in EtOH.[18] In addition, Thomas and coworkers reported formation of a $Co^{I}$ species in a heterobimetallic Zr/Co system upon metallation of $[(R_2PNR')_3Zr(Cl)]$ (where R = Ph, $^{i}$Pr; R′ = $^{i}$Pr, Mes) with $CoI_2$.[23] The authors noted $I^-$ as the likely reducing agent in both cases, with $I_2$ generated as byproduct. Consistent with this proposal, metalation of PhP3 with $CoBr_2$ in place of $CoI_2$ produced a violet solution, similar to the blue color of μ-$(Cl)_2$-$[\{(MeP3)Co^{II}\}_2]$ reported by Schober.[19a]

## Electrochemistry

In cyclic voltammetry (CV) experiments, **1** in THF exhibits an oxidation wave at +0.38 V *vs.* SCE ($Fc/Fc^+$ as internal standard, Pt WE), which we assign to $Co^{I} \rightarrow Co^{II}$ oxidation. In the subsequent cathodic sweep, reduction of this species occurs at −0.51 V; this reduction wave is not observed without first proceeding through the $Co^{I} \rightarrow Co^{II}$ oxidation. Both $Co^{II/I}$ reactions exhibit scan rate dependences (Fig. 2, inset) consistent with diffusion controlled processes, suggesting that the large peak-to-peak separation is not due to electrode adsorption. No

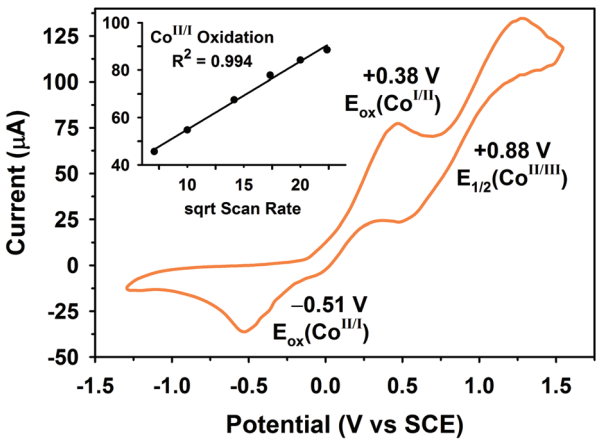


**Fig. 2** Cyclic voltammogram of **1** under an Ar atmosphere in THF solution with 0.1 M $NEt_4ClO_4$: scan rate, 200 mV $s^{-1}$; WE, Pt; RE, $Ag/AgNO_3$ in MeCN; CE, Pt.

further $Co^{I/0}$ reduction occurs in the range 0 to −1.5 V, but a quasi-reversible $Co^{III/II}$ couple is observed at +0.88 V.

It is unusual that the $Co^{I/II}$ oxidation occurs at a positive potential *versus* SCE. For example, the closely related [(MeP3)-$Co^{I}$(Cl)] (prepared *via* reduction of $[(MeP3)Co^{II}(Cl)_2]$ with $BH_3$·THF) is oxidized near 0 V *vs.* SCE),[19a] which is 400 mV positive of the oxidation of **1**. In another case, formation of $[(NP3)Co^{I}(Br)]$ from its $Co^{II}$ precursor was achieved using $NaBH_4$ ($E_0 \approx -1.2$ V) in DMF.[16] As noted earlier, Sacconi observed formation of $[(MeP3)Co^{I}(I)]$ in refluxing $CH_2Cl_2$–EtOH;[19a] however, the $Co^{II/I}$ potentials for this system were not reported. In our system, contributions to the more positive potential include exchange of $Cl^-$ for $I^-$, as well as substitution of the methyl group in MeP3 for the more electron withdrawing phenyl anchor in PhP3.

The formation of the $Co^{I}$ complex presumably occurs *via* oxidation of $I^-$: $Co^{II} + I^- \rightarrow Co^{I} + 1/2\ I_2$. The oxidation potential of iodide in polar organic solvents such as MeCN or THF is less positive (+0.25 V *vs.* SCE) than the $E_{ox}$ for **1** (+0.38 V), thus accounting for spontaneous redox reaction. In our system, we were unable to detect the presence of $I_2$ in the reaction (starch test). We also did not observe catalytic oxidation of $I^-$ in CVs of **1** in presence of excess $I^-$ (10 mM).

## UV/vis/NIR absorption spectrum

The UV/vis absorption spectrum of **1** in THF (Fig. 3) exhibits a strong feature at 320 nm ($\varepsilon$ = 8970 $M^{-1}$ $cm^{-1}$) and a weak absorption at 850 nm ($\varepsilon$ = 240 $M^{-1}$ $cm^{-1}$). We assign the 320 nm absorption as d(Co) → $\pi^*(PPh_2)$ MLCT, and the lower intensity 850 nm feature as a d–d transition. The orange solution of **1** is similar to the yellow color observed for $[(MeP3)Co^{I}(Cl)]$, but quite distinct from the blue-green color of structurally related $[(PPh_3)_3Co^{I}(Cl)]$ ($\lambda_{max}$ = 680 nm),[32,47] wherein the lack of steric strain results in a more ideal tetrahedral geometry (Cl–Co–$P_{avg}$ = 114°)[12] *versus* the distorted geometry of **1** (I–Co–$P_{avg}$ = 124.2°). Exposure of a solution of **1** in THF to oxygen leads to a rapid change in color from orange to pale blue, indicating formation of a $Co^{II}$ species (*vide infra*, EPR section), similar to a report of the reaction of $[(PPh_3)_3Co(Cl)]$ in air.[32] The change in color is accompanied by a decrease in the intensities of both the MLCT band at 320 nm and the d–d feature at 850 nm. A concomitant increase in absorption at 680 nm is observed, logically attributable to a d–d transition in the spectrum of the $Co^{II}$ product.

An absorption feature extending beyond 1100 nm was initially observed, but it was not resolved by standard UV/vis spectrophotometry. Therefore, we also present the NIR absorption features of **1** in $d^8$-THF solution (in the bottom panel of Fig. 3, the corresponding 850 nm band is shown at 11 500 $cm^{-1}$). As a benchmark, we compare the absorption spectrum of **1** to the isoelectronic complex $[Ni^{II}(Cl)_4]^{2-}$. This complex has been examined in single crystal form to determine transition energies and band assignments,[48] as well as in organic solvents for quantification of band intensities.[49] Tetrachloronickelate(II) exhibits a visible absorption band near 14 700 $cm^{-1}$ (Table 3) that is of similar intensity ($\varepsilon$ = 200 to 350 $M^{-1}$ $cm^{-1}$) to that of the 11 500 $cm^{-1}$ feature of **1** ($\varepsilon$ = 230 $M^{-1}$ $cm^{-1}$), but, unlike the weak NIR absorption at 7300 $cm^{-1}$ ($\varepsilon \approx 30$ $M^{-1}$ $cm^{-1}$) in

the $[Ni(Cl)_4]^{2-}$ solution spectrum, **1** exhibits a more intense absorption that is split into two well-separated features: a peak at 8650 $cm^{-1}$ ($\varepsilon$ = 450 $M^{-1}$ $cm^{-1}$) and a prominent shoulder at 7950 $cm^{-1}$ ($\varepsilon$ = 430 $M^{-1}$ $cm^{-1}$).

Aresta *et al.*[47] and Telser *et al.*[32] have previously undertaken an analysis of the vis/NIR absorption spectra of geometry-unconstrained (P3)$Co^{I}$(X) compounds, in particular $[(PPh_3)_3Co^{I}(Cl)]$. (Note: neither group investigated their absorptions in solution at $\lambda$ > 1100 nm; we circumvented this limitation by using $d^8$-THF.) The unconstrained complex $[(PPh_3)_3Co^{I}(Cl)]$ exhibits absorption features at energies (13 500, 10 400, 9050 $cm^{-1}$) that are similar to those of $[Ni(Cl)_4]^{2-}$ (14 700, 12 100, 7270 $cm^{-1}$).[48] However, the tris(triarylphosphine) complex, $[(PPh_3)_3Co^{I}(Cl)]$, exhibits a more closely spaced pattern of features (three prominent vis/NIR features) that is, in fact, more like those of **1**. On the basis of previous assignments for the $C_{3v}$ $^3A_2$ ground state, we assign the ligand field transitions as $^3A_2 \rightarrow {}^3E$ [11 500 $cm^{-1}$]; $^3A_2 \rightarrow {}^3A_2$ [8650 $cm^{-1}$]; and $^3A_2 \rightarrow {}^3A_2$ [7950 $cm^{-1}$]. Overall, we conclude from the position of the highest energy transition [$^3A_2 \rightarrow {}^3E$; 11 500 $cm^{-1}$] that the strained geometry of the (P3)Co(X) unit in **1** (due to coordinated PhP3) generates an overall weaker ligand field, so the LF order is $[Ni(Cl)_4]^{2-}$ > $[(PPh_3)_3Co^{I}(Cl)]$ > [(PhP3)$Co^{I}$(I)] (**1**) [see DFT section].

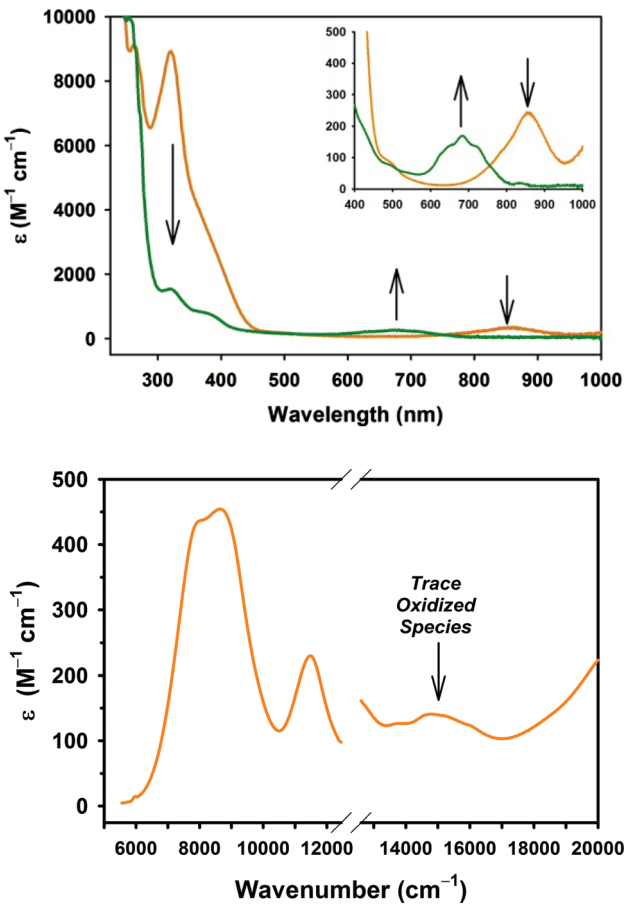


**Fig. 3** *Top*: UV/vis absorption spectrum of complex **1** under $N_2$ in THF at 298 K (orange line), and after exposure to air (green line). *Inset*: Magnified view of the low energy region. *Bottom*: Vis/NIR absorption spectrum of **1** in $d^8$-THF under $N_2$ atmosphere.

### Magnetic properties (solid state)

To confirm the $Co^{I}$ oxidation state as suggested by the crystal structure of **1**, we employed temperature dependent magnetometry (SQUID). As shown in Fig. 4, a polycrystalline sample of **1** exhibits $\mu_{eff}$ = 2.99(6) $\mu_B$ in the temperature range 20–300 K (5000 G), which is close to the expected $S$ = 1 spin-only value (2.83 $\mu_B$). Several related complexes in (P3)$Co^{I}$(X) ligation have displayed similar $\mu_{eff}$ values based on solid state measurements.[15a,16b,18,19a,50] Least squares fitting (julX)[51] of the low temperature data (4–50 K) suggests a zero-field splitting $|D|$ = 8 $cm^{-1}$ in the solid state, which is at the high end of the range of values attributed to $[(PPh_3)_3Co(X)]$ (X = Cl, Br) in solution studies.[32]

### EPR spectroscopy

The non-Kramers ground state of **1** rendered observation of a spectroscopic signature in conventional EPR spectroscopy (perpendicular mode, X-band) unlikely. In related work, Telser and coworkers reported the HFEPR spectra of $[(PPh_3)_3Co(X)]$ (X = Cl, Br) at 406 GHz (40 000–120 000 G) in perpendicular mode.[32] Utilizing parallel mode EPR, Britt and coworkers have detected signals at conventional frequencies/fields (X-band) from several biologically relevant integer-spin systems such as Mn-SOD and photoxidized photosystem II.[33,34] Hendrich and coworkers also have established the utility of parallel mode EPR measurements in antiferromagnetically coupled integer spin systems in both protein[37] and small molecule[38] environments. In closely related work, several *trigonal* integer spin systems such as [(H3buea)$Fe^{IV}$(O)]$^-$ ($S$ = 2), [(H3buea)$Mn^{III}$(O)]$^{2-}$ ($S$ = 2) and [(H3buea)$Mn^{V}$(O)] ($S$ = 1), which have been reported by Borovik *et al.*,[35,36] also exhibit parallel mode features at conventional magnetic field strengths (0–5000 G). On this basis, identification of a parallel mode signature for our trigonal $Co^{I}$ complex seemed feasible. The parallel mode EPR spectrum

**Table 3** Comparison of vis/NIR features in pseudotetrahedral $d^8$ complexes

| Complex | Transition in $cm^{-1}$ [assignment] | | | Ref. |
|---|---|---|---|---|
| $[Ni^{II}(Cl)_4]^{2-}$ | 14 700 [$^3T_1$(F) → $^3T_1$(P)] | 12 100 [$^3T_1$(F) → see[a]] | 7270 [$^3T_1$(F) → $^3A_2$(F)] | 48 |
| $[(PPh_3)_3Co^{I}(Cl)]$ | 13 500 [$^3A_2 \rightarrow {}^3E$] | 10 400 [$^3A_2 \rightarrow {}^3A_2$] | 9050 [$^3A_2 \rightarrow {}^3A_2$] | 32 |
| [(PhP3)Co(I)] (**1**) | 11 500 [$^3A_2 \rightarrow {}^3E$] | 8650 [$^3A_2 \rightarrow {}^3A_2$] | 7950 [$^3A_2 \rightarrow {}^3A_2$] | This work |

[a] Forbidden transition to a closely spaced $^1T_2$(D), $^1E$(D) pair.

 

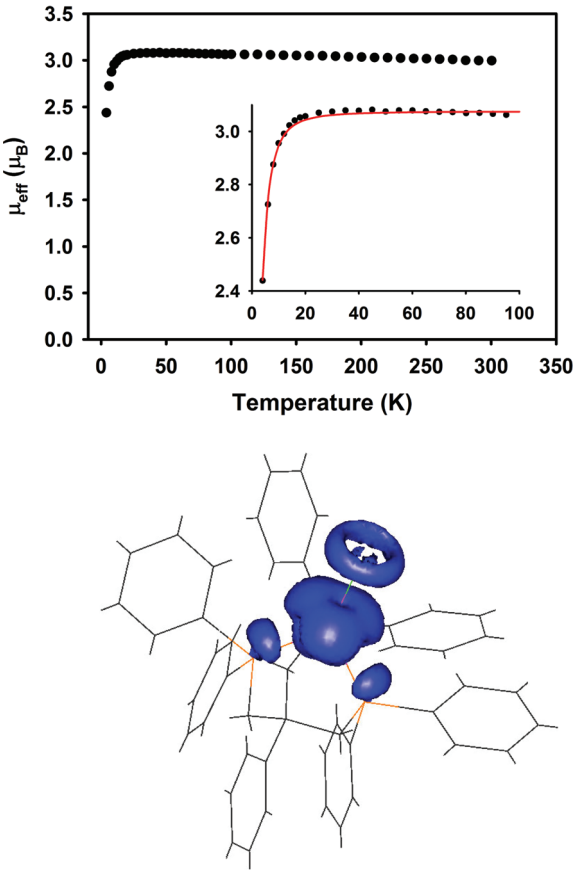


**Fig. 4** *Top*: Magnetic susceptibility (●) of **1** recorded from 4 to 300 K. *Inset*: Magnified view of SQUID data (●) and best fit regression (—) from 4 to 100 K of susceptibility data; fit parameters: $|D| = 8$ cm$^{-1}$, $g_{eff} = 2.17$ (julX). *Bottom*: DFT calculated spin density plot (Firefly: PW91/6-31G*) for the geometry optimized coordinates of **1**.

(X-band) of **1** in THF/toluene (1 : 1) frozen glass at 4 K is shown in Fig. 5 (upper left). The spectrum consists of a sharp feature at $g = 4.16$, and a broad continuous absorption from 2500 to 15 000 G (see background scan, Fig. 5, upper left). We did not observe Co ($I = 7/2$) hyperfine features at various temperatures (4–125 K), microwave powers (0.1–10 mW), or concentrations (0.1–100 mM). We note, however, that the presence of $^{59}$Co, three $^{31}$P and $^{127}$I (all nearly 100% abundant) may render the hyperfine features unobservable at the resolution of the spectrometer (in X-band). The observed forbidden $\Delta m = 2$ signal in parallel mode may be enhanced by deviations from strict $C_{3v}$ geometry in solution (*e.g.* $E/D \approx 0.01$).

To ensure that the observed feature at $g = 4.16$ was attributable to Co$^{I}$ (and not trace Co$^{II}$), we investigated the change in EPR spectra (parallel and perpendicular modes) upon exposure of the THF/toluene solution of **1** to air. Exposure to air results in a rapid color change from orange to pale green-blue (*vide supra*, UV/vis section). Fig. 5 (right side) shows that upon exposure to air, the loss of signal at $g = 4.16$ in the parallel mode spectrum is accompanied by a concomitant increase in features in the perpendicular mode spectrum ($g = 5.55$, 2.13) attributable to the formation of Co$^{II}$ (bottom panels).

The presence of trace amounts of Co$^{II}$ (perpendicular mode: features at $g = 5.55$, 2.13) in THF/toluene under 'anaerobic' conditions ($N_2$ drybox) was of some concern: this prompted us to examine EPR spectra of **1** in the solid state. Polycrystalline **1** exhibits an analogous (yet predictably less intense) feature in parallel mode at $g \approx 3.5$ (Fig. 6). The corresponding perpendicular mode spectrum *exhibits no features*, consistent with pure Co$^{I}$ material in the solid state. We therefore attribute the trace Co$^{II}$ features in the perpendicular mode spectrum of **1** in THF/toluene to reaction of **1** with trace dioxygen (or peroxides) present in our THF solvent (a reaction that occurs on a much slower time scale in the solid state). Overall, Fig. 7 summarizes the Zeeman splitting diagram consistent with the experimental data for **1**.

### DFT calculations and electronic structure

We performed DFT calculations employing the X-ray coordinates of **1** for the $S = 1$ and $S = 0$ configurations (without symmetry constraints in both cases). All calculations indicate that the high-spin ($S = 1$) ground state is ~10 kcal mol$^{-1}$ lower in energy than the singlet configuration. In the DFT optimized geometry of **1** ($S = 1$), the electron density of the highest SOMO is delocalized over the Co and I atoms (Fig. 8, middle); Analogous calculations on the DFT-optimized structure of the putative complex [(PhP3)Co(Cl)] (data not shown) showed similar delocalization of SOMO density onto the Cl$^-$ ligand, possibly suggesting a change from Cl$^-$ to I$^-$ is not responsible for the drastic change in oxidation potential. The DFT calculated spin density plot (Fig. 4 bottom) shows that the triplet spin is located primarily at the metal center, indicating that PhP3 ligand is 'innocent', *i.e.* devoid of radical character.

Although the 6-31G*/PW91 optimized structure agreed in most respects with the X-ray coordinates (Table 2), a slight opening (greater than ~2°) of the P–Co–P bond angles (93.03, 92.60, 91.33°) compared to the crystal structure (P–Co–$I_{avg}$ = 91.7(7)) was of some concern. Closer analysis of the DFT calculations on **1** with several basis sets (6-31G*, TZV) and functionals (PW91, B3PW91) reveals varying extents of agreement with the X-ray structure. While both the TZV/PW91 and 6-31G*/B3PW91 calculations more faithfully reproduced the experimentally observed P–Co–P angles (avg = 91.2(8), 92.3(9)° respectively), they also led to unacceptable errors in the Co–P distances (2.286(1), 2.240(2) Å) *versus* the X-ray parameters (Co–$P_{avg}$ = 2.215(12) Å). At one extreme, the TZV/B3PW91 calculation favors an *asymmetric* ground state with regards to Co–P distances (2.441, 2.431, 2.322 Å) and P–Co–I angles (123.2, 124.8, 127.6°). Consistent with this finding, the singly occupied α and β orbitals are at drastically different energies (−1.877, −2.150 eV) within the TZV/B3PW91 calculated orbital set. In contrast, the structurally relevant 6-31G*/PW91 calculation favors a more symmetric ground state structure (Co–P = 2.188, 2.192, 2.192 Å) with nearly identical α and β orbital energies (−3.812, −3.813 eV). While a small extent of asymmetry is present in the experimental data for both **1** (Co–P = 2.1953(14), 2.2052(14), 2.2219(14) Å) and **1′** (2.2239(12), 2.2259(13), 2.2160(13) Å), such deviations are within a range that could be attributable to crystal packing rather than a difference in ground state electronic structure, as would be suggested by the TZV/B3PW91 calculation. Interestingly, [$(PPh_3)_3$Co(Cl)] crystallizes

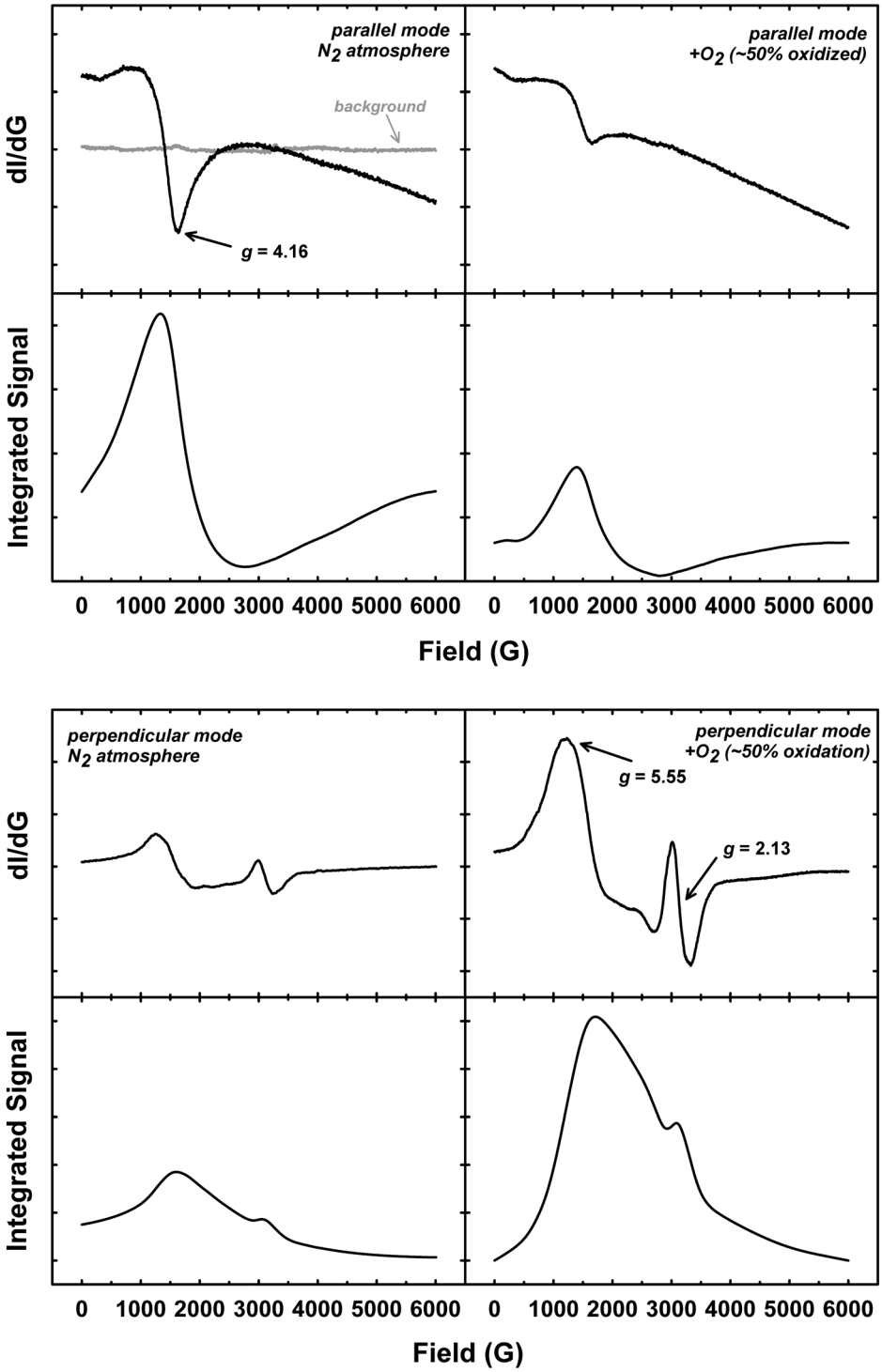


**Fig. 5** Parallel mode (top four panels) and perpendicular mode (bottom four panels) X-band EPR spectra of **1** in THF/toluene (1 : 1) frozen glass at 10 K. *Left side*: sample prepared under $N_2$; *right side*: sample exposed to air for several minutes at 298 K. No features were observed in the region 6000–15 000 G. Instrument parameters: microwave frequency, 9.40 GHz (parallel), 9.60 GHz (perpendicular); microwave power, 10 mW; modulation frequency, 100 kHz; modulation amplitude, 4 G.

in discrete conformers that may be attributable to such asymmetric ground states.[32]

Taken together, the structural, magnetic and vis/NIR properties coupled with DFT calculations allow us to characterize the electronic structure of **1**, which is summarized in Fig. 8. The DFT calculated orbital energies (6-31G*/PW91) are consistent with a triplet ground state, with low-lying *xy* and $x^2 - y^2$ orbitals (equivalent in $C_{3v}$), and $z^2$ is a doubly occupied orbital of intermediate energy; the equivalent SOMOs are dominated by the *xz* and *yz* orbitals. In a qualitative sense, this electronic structure

 

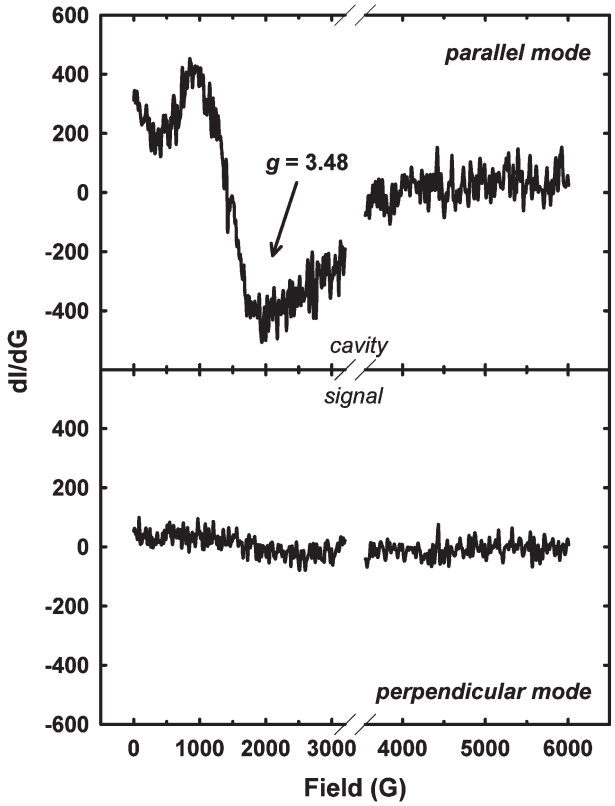


**Fig. 6** Parallel mode (top panel) and perpendicular mode (bottom panel) X-band EPR spectra of polycrystalline **1** (solid sample) at 10 K. No features were observed in the range 6000–15 000 G. Instrument parameters: microwave frequency, 9.40 GHz (parallel), 9.60 GHz (perpendicular); microwave power, 10 mW; modulation frequency, 100 kHz; modulation amplitude, 4 G.

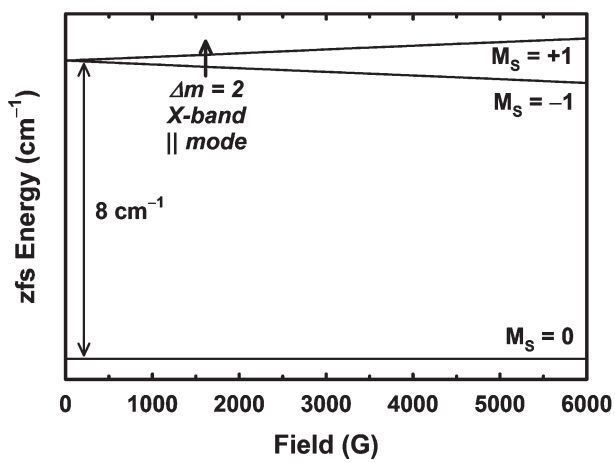


**Fig. 7** *Top*: Energy levels and Zeeman splitting for **1**, using parameters consistent with SQUID and EPR studies: $S = 1$; $|D| = 8$ cm$^{-1}$; $E/|D| = 0$; $g_{eff} = 2.17$ (Note: $g_{eff}$ here represents the magnetic susceptibility coefficient.)

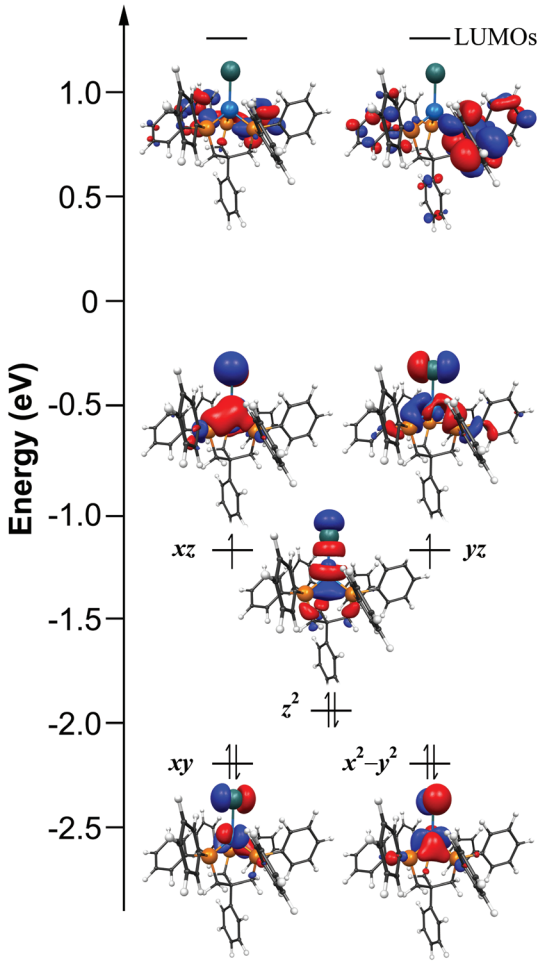


**Fig. 8** *Left*: Energy diagram for **1** calculated by DFT (PW91/6-31G*), including metal-based occupied MOs and ligand-based LUMOs. (Note: energy scale has been arbitrarily set to 0 eV between the SOMO and LUMO; assignments of *xy versus* $x^2 - y^2$, and *xz versus yz* are arbitrary.)

description is in agreement with that for a number of (P3)Co(X) complexes.[32] In particular, we wish to point out some observations regarding the calculated orbital energies as compared to the experimentally documented vis/NIR transitions. As can be seen in Fig. 8, ligand field transitions could be expected at approximately 7800, 5200 and 2580 cm$^{-1}$ (note that the lowest energy transition is well outside the accessible solvent/instrument window). Experimentally, **1** exhibits a single transition at 11 760 cm$^{-1}$, while the feature at lower energy is observed as a split system centered near 8250 cm$^{-1}$. It is possible that this split transition is observed due to a portion of **1** in a non-$C_{3v}$ geometry in solution; such a geometry is not accounted for by the 6-31G*/PW91 calculation summarized in Fig. 8. The plausibility of such a species is suggested by both the DFT calculations (6-31G*/B3PW91, TZV/B3PW91) and the discrete structural conformers observed for $[(PPh_3)_3Co(Cl)]$.[32] A more detailed TD-DFT study (beyond the scope of this work) on each configuration may give insight as to the relative contributions of each geometry to the experimentally observed spectrum.

## Conclusion

We have observed spontaneous formation of a $Co^{I}$-iodo species from $CoI_2$ starting material. The resulting $Co^{I}$ complex,

[(PhP3)Co$^{I}$(I)] (**1**), which has been structurally characterized by X-ray diffraction, exhibits Co$^{I/II}$ oxidation at a positive potential *vs.* SCE (+0.4 V). Parallel mode EPR experiments provide a spectroscopic signature for high-spin, trigonal Co$^{I}$ (or other d$^{8}$) species that should be useful to other investigators.

## Acknowledgements

We thank Larry Henling and the late Michael Day for X-ray data collection and crystal structure refinement. We gratefully acknowledge Markus Ribbe (UC Irvine) for generous use of a dual mode EPR cavity. Our work was supported by the NSF CCI Solar Fuels program (CHE-0802907) and by CSER (Gordon and Betty Moore Foundation); MJR acknowledges an ACC-F postdoctoral fellowship from the NSF (CHE-1042009). DEB thanks the Rossum family for a SURF award. The Bruker KAPPA APEXII X-ray diffractometer was purchased *via* an NSF CRIF:MU award to the California Institute of Technology (CHE-0639094).



## References

1 (*a*) A. Arevalo and J. J. Garcia, *Eur. J. Inorg. Chem.*, 2010, 4063–4074; (*b*) A. Furstner, K. Majima, R. Martin, H. Krause, E. Kattnig, R. Goddard and C. W. Lehmann, *J. Am. Chem. Soc.*, 2008, **130**, 1992–2004.
2 (*a*) Z. Lian, X. F. Xu, H. J. Sun, Y. Chen, T. T. Zheng and X. Y. Li, *Dalton Trans.*, 2010, **39**, 9523–9529; (*b*) T. T. Zheng, H. J. Sun, Y. Chen, X. Y. Li, S. Durr, U. Radius and K. Harms, *Organometallics*, 2009, **28**, 5771–5776; (*c*) N. Satyanarayana and M. Periasamy, *J. Organomet. Chem.*, 1987, **333**, C33–C36; (*d*) J. Clemens, M. Green and F. G. A. Stone, *J. Chem. Soc., Dalton Trans.*, 1974, 93–97.
3 R. Poli, *Chem. Rev.*, 1996, **96**, 2135–2204.
4 (*a*) Y. Li and W. T. Wong, *Coord. Chem. Rev.*, 2003, **243**, 191–212; (*b*) B. H. S. Thimmappa, *Coord. Chem. Rev.*, 1995, **143**, 1–34.
5 (*a*) C. G. Riordan, *Coord. Chem. Rev.*, 2010, **254**, 1815–1825; (*b*) J. A. DuPont, G. P. A. Yap and C. G. Riordan, *Inorg. Chem.*, 2008, **47**, 10700–10707.
6 (*a*) R. J. Klingler, M. J. Chen, J. W. Rathke and K. W. Kramarz, *Organometallics*, 2007, **26**, 352–357; (*b*) M. Beller, B. Cornils, C. D. Frohning and C. W. Kohlpainter, *J. Mol. Catal. A: Chem.*, 1995, **104**, 17–85; (*c*) G. W. Parshall and S. D. Ittle, *Homogeneous Catalysis*, Wiley-Interscience, New York, 1992; (*d*) J. P. Collman, L. S. Hegedus, J. R. Norton and R. G. Finke, *Principles and Applications of Organotransition Metal Chemistry*, University Science Books, Mill Valley, CA, 1987.
7 (*a*) M. Lombardo, A. Gualandi, F. Pasi and C. Tromobini, *Adv. Synth. Catal.*, 2007, **349**, 465–468; (*b*) G. R. Pettit and M. P. Grealish, *J. Org. Chem.*, 2001, **66**, 8640–8642; (*c*) F. Orsini, M. Pulici and L. M. Vallarino, *J. Organomet. Chem.*, 1995, **495**, C1–C5.
8 (*a*) Y. Sugiyama and S. Okamoto, *Synthesis*, 2011, **14**, 2247–2254; (*b*) G. Hilt, A. Paul and J. Treutwein, *Org. Lett.*, 2010, **12**, 1536–1539; (*c*) C. Aubert, P. Betschmann, M. J. Eichberg, V. Gandon, T. J. Heckrodt, J. Lehmann, M. Malacria, B. Masjost, E. Paredes, K. P. C. Vollhardt and G. D. Whitener, *Chem.–Eur. J.*, 2007, **13**, 7443–7465; (*d*) M. J. Eichberg, R. L. Dorta, D. B. Grotjahn, K. Lamottke, M. Schmidt and K. P. C. Vollhardt, *J. Am. Chem. Soc.*, 2001, **123**, 9324–9337.
9 (*a*) T. M. Kooistra, Q. Knijnenburg, J. M. M. Smits, A. D. Horton, P. H. M. Budzelaar and A. W. Gal, *Angew. Chem., Int. Ed.*, 2001, **40**, 4719–4722; (*b*) H.-F. Klein, R. Hammer, J. Gross and U. Schubert, *Angew. Chem., Int. Ed. Engl.*, 1980, **19**, 809–810.
10 K. Gao, P.-S. Lee, T. Fujita and N. Yoshikai, *J. Am. Chem. Soc.*, 2010, **132**, 12249–12251.
11 P. S. Lin, M. Jeganmohan and C.-H. Cheng, *Chem.–Eur. J.*, 2008, **14**, 11296–11299.
12 J. M. Cassidy and K. H. Whitmire, *Acta Crystallogr., Sect. C: Cryst. Struct. Commun.*, 1991, **47**, 2094.
13 C. Y. Dai, G. Stringer, J. F. Corrigan, N. J. Taylor, T. B. Marder and N. C. Norman, *J. Organomet. Chem.*, 1996, **513**, 273.
14 J. A. Bandy, J. C. Green and O. N. Kirchner, *Acta Crystallogr., Sect. C: Cryst. Struct. Commun.*, 1985, **41**, 1179.
15 (*a*) M. Aresta, M. Rossi and A. Sacco, *Inorg. Chim. Acta*, 1969, **3**, 227–231; (*b*) A. Sacco and M. Rossi, *Inorg. Chim. Acta*, 1968, **2**, 127.
16 (*a*) C. A. Ghilardi, C. Mealli, S. Midollini and A. Orlandini, *Inorg. Chem.*, 1985, **24**, 164–168; (*b*) L. Sacconi, C. A. Ghilardi and F. Zanobini, *Inorg. Chem.*, 1975, **14**, 1380–1386.
17 C. A. Ghilardi, S. Midollini and L. Sacconi, *Inorg. Chem.*, 1975, **14**, 1790–1795.
18 L. Sacconi and S. Midollini, *J. Chem. Soc., Dalton Trans.*, 1972, 1213–1216.
19 (*a*) K. Heinze, G. Huttner, L. Zsolnai and P. Schober, *Inorg. Chem.*, 1997, **36**, 5457–5469; (*b*) F. Karadas, E. J. Schelter, M. Shatruk, A. V. Prosvirin, J. Basca, D. Smirnov, A. Ozarowski, J. Krzystek, J. Telser and K. R. Dunbar, *Inorg. Chem.*, 2008, **47**, 2074–2082; (*c*) R. Rupp, A. Frick, G. Huttner, P. Rutsch, U. Winterhalter, A. Barth, P. Kirchner and L. Zsolnai, *Eur. J. Inorg. Chem.*, 2000, 523–536; (*d*) U. Winterhalter, L. Zsolnai, P. Kirchner, K. Heinze and G. Huttner, *Eur. J. Inorg. Chem.*, 2001, 89–103.
20 (*a*) D. M. Jenkins and J. C. Peters, *J. Am. Chem. Soc.*, 2005, **127**, 7148–7165; (*b*) D. M. Jenkins and J. C. Peters, *J. Am. Chem. Soc.*, 2003, **125**, 11162–11163; (*c*) D. M. Jenkins, A. J. Di Bilio, M. J. Allen, T. A. Betley and J. C. Peters, *J. Am. Chem. Soc.*, 2002, **124**, 15336–15350; (*d*) D. M. Jenkins, T. A. Betley and J. C. Peters, *J. Am. Chem. Soc.*, 2002, **124**, 11238–11239; (*e*) I. R. Shapiro, D. M. Jenkins, J. C. Thomas, M. W. Day and J. C. Peters, *Chem. Commun.*, 2001, 2152–2153.
21 (*a*) A. Takaoka and J. C. Peters, *Inorg. Chem.*, 2012, **51**, 16–18; (*b*) M. T. Whited, N. P. Mankad, Y. Lee, P. F. Oblad and J. C. Peters, *Inorg. Chem.*, 2009, **48**, 2507–2517.
22 T. A. Betley and J. C. Peters, *Inorg. Chem.*, 2003, **42**, 5074–5084.
23 (*a*) J. P. Krogman, B. M. Foxman and C. M. Thomas, *J. Am. Chem. Soc.*, 2011, **133**, 14582–14585; (*b*) B. P. Greenwood, S. I. Forman, G. T. Rowe, C.-H. Chen, B. M. Foxman and C. M. Thomas, *Inorg. Chem.*, 2009, **48**, 6251–6260.
24 M. Alajarín, C. López-Leonardo, J. Berná and J. W. Steed, *Tetrahedron*, 2007, **63**, 2078–2083.
25 (*a*) L. Beaufort, L. Delaude and A. F. Noels, *Tetrahedron*, 2007, **63**, 7003–7008; (*b*) N. Röckendorf, O. Sperling and T. K. Lindhorst, *Aust. J. Chem.*, 2002, **55**, 87–93; (*c*) R. Viguier, G. Serratrice, A. Dupraz and C. Dupuy, *Eur. J. Inorg. Chem.*, 2001, 1789–1795.
26 D. H. Kim, J. H. Park and S. D. Cho, *J. Korean Chem. Soc.*, 1992, **36**, 163–164.
27 (*a*) E. I. Solomon, T. C. Brunold, M. I. Davis, J. N. Kemsley, S.-K. Lee, N. Lehnert, F. Neese, A. J. Skulan, Y.-S. Yang and J. Zhou, *Chem. Rev.*, 2000, **100**, 235–349; (*b*) J. Du, M. Sono and J. H. Dawson, *Coord. Chem. Rev.*, 2011, **255**, 700–716; (*c*) J. McMaster and V. S. Oganesyan, *Curr. Opin. Struct. Biol.*, 2010, **20**, 615–622.
28 (*a*) R. E. Linder and J. R. Rowlands, *Spectrosc. Lett.*, 1971, **4**, 227; (*b*) P. J. Stephens, *Annu. Rev. Phys. Chem.*, 1974, **25**, 201–232; (*c*) B. E. Williamson, T. C. VanCott, M. E. Boyle, G. C. Misener, M. J. Stillman and P. N. Schatz, *J. Am. Chem. Soc.*, 1992, **114**, 2412–2419.
29 (*a*) S. H. Choi, J. A. Phillips, W. Ware, C. Wittschieben, C. J. Medforth and K. M. Smith, *Inorg. Chem.*, 1994, **33**, 3873–3876; (*b*) P. E. M. Siegbahn, J. W. Tye and M. Hall, *Chem. Rev.*, 2007, **107**, 4414–4435.
30 S. Vongtragool, B. Gorshunov, M. Dressel, J. Krzystek, D. M. Eichhorn and J. Telser, *Inorg. Chem.*, 2003, **42**, 1788–1790.
31 (*a*) P. J. Desrochers, C. A. Sutton, M. L. Abrams, S. Ye, F. Neese, J. Telser, A. Ozarowski and J. Krzystek, *Inorg. Chem.*, 2012, **51**, 2793–2805; (*b*) I. Nieto, R. P. Bontchev, A. Ozarowski, D. Smirnov, J. Krzystek, J. Telser and J. M. Smith, *Inorg. Chim. Acta*, 2009, **362**, 4449–4460; (*c*) P. J. Desrochers, J. Telser, S. A. Zvyagin, A. Ozarowski, J. Krzystek and D. A. Vicic, *Inorg. Chem.*, 2006, **45**, 8930–8941; (*d*) J. Krzystek, J.-H. Park, M. W. Meisel, M. A. Hitchman, H. Stratemeier, L.-C. Brunel and J. Telser, *Inorg. Chem.*, 2002, **41**, 4478–4487.
32 J. Krzystek, A. Ozarowski, S. A. Zvyagin and J. Telser, *Inorg. Chem.*, 2012, **51**, 4954–4964.
33 (*a*) K. A. Campbell, J. M. Peloquin, D. P. Pham, R. J. Debus and R. D. Britt, *J. Am. Chem. Soc.*, 1998, **120**, 447–448; (*b*) K. A. Campbell, D. A. Force, P. J. Nixon, F. Dole, B. A. Diner and R. D. Britt, *J. Am. Chem. Soc.*, 2000, **122**, 3754–3761; (*c*) R. D. Britt, J. M. Peloquin and K. A. Campbell, *Annu. Rev. Biophys. Biomol. Struct.*, 2000, **29**, 463–495;

 

(*d*) K. A. Campbell, M. R. Lashley, J. K. Wyatt, M. H. Nantz and R. D. Britt, *J. Am. Chem. Soc.*, 2001, **123**, 5710–5719.
34 K. A. Campbell, E. Yikilmaz, C. V. Grant, W. Gregor, A.-F. Miller and R. D. Britt, *J. Am. Chem. Soc.*, 1999, **121**, 4714–4715.
35 D. C. Lacy, R. Gupta, K. L. Stone, J. Greaves, J. W. Ziller, M. P. Hendrich and A. S. Borovik, *J. Am. Chem. Soc.*, 2010, **132**, 12188.
36 (*a*) T. H. Parsell, R. K. Behan, M. T. Green, M. P. Hendrich and A. S. Borovik, *J. Am. Chem. Soc.*, 2006, **128**, 8728; (*b*) T. Taguchi, R. Gupta, B. Lassalle-Kaiser, D. W. Boyce, V. K. Yachandra, W. B. Tolman, J. Yano, M. P. Hendrich and A. S. Borovik, *J. Am. Chem. Soc.*, 2012, **134**, 1996; (*c*) R. L. Shook, W. A. Gunderson, J. Greaves, J. W. Ziller, M. P. Hendrich and A. S. Borovik, *J. Am. Chem. Soc.*, 2008, **130**, 8888–8889.
37 (*a*) M. M. Mbughuni, M. Chakrabarti, J. A. Hayden, K. K. Meier, J. J. Dalluge, M. P. Hendrich, E. Munck and J. D. Lipscomb, *Biochemistry*, 2011, **50**, 10262–10275; (*b*) M. M. Mbughini, M. Chakrabarti, J. A. Hayden, E. L. Bominaar, M. P. Hendrich, E. Munck and J. D. Lipscomb, *Proc. Natl. Acad. Sci. U. S. A.*, 2010, **107**, 16788–16793; (*c*) B. S. Pierce, T. E. Elgren and M. P. Hendrich, *J. Am. Chem. Soc.*, 2003, **125**, 8748–8759; (*d*) A. K. Upadhyay, D. T. Petasis, D. M. Arciero, A. B. Hooper and M. P. Hendrich, *J. Am. Chem. Soc.*, 2003, **125**, 1738–1747.
38 A. P. Golombek and M. P. Hendrich, *J. Magn. Reson.*, 2003, **165**, 33–48.
39 A. B. Pangborn, M. A. Giardello, R. H. Grubbs, R. K. Rosen and F. J. Timmers, *Organometallics*, 1996, **15**, 1518–1520.
40 O. Kahn, *Molecular Magnetism*, VCH Publishers, New York, 1993.
41 (*a*) J. P. Perdew, J. A. Chevary, S. H. Vosko, K. A. Jackson, M. Pederson, D. J. Singh and C. Fiolhais, *Phys. Rev. B: Condens. Matter*, 1993, **48**, 4978; (*b*) J. P. Perdew, J. A. Chevary, S. H. Vosko, K. A. Jackson, M. R. Pederson, D. J. Singh and C. Fiolhais, *Phys. Rev. B: Condens. Matter*, 1992, **46**, 6671–6687.
42 (*a*) A. D. Becke, *J. Chem. Phys.*, 1993, **98**, 5648; (*b*) P. J. Stephens, F. J. Devlin, C. F. Chabalowski and M. J. Frisch, *J. Phys. Chem.*, 1994, **98**, 11623–11627.
43 A. A. Granovsky, *Firefly v.7.1*, http://classic.chem.msu.su/gran/firefly/index.html
44 B. M. Bode and M. S. Gordon, *J. Mol. Graphics Modell.*, 1998, **16**, 133–138.
45 (*a*) L. Laaksonen, *J. Mol. Graphics Modell*, 1992, **10**, 33–34; (*b*) D. L. Bergman, L. Laaksonen and A. Laaksonen, *J. Mol. Graphics Modell.*, 1997, **15**, 301–306.
46 C. Mealli, P. L. Orioli and L. Sacconi, *J. Chem. Soc. A*, 1971, 2691.
47 M. Aresta, M. Rossi and A. Sacco, *Inorg. Chim. Acta*, 1969, **3**, 227–231.
48 V. J. Koester and T. M. Dunn, *Inorg. Chem.*, 1975, **14**, 1811–1817.
49 A. Chiboub-Fellah, J. Meullemeestre, C. Spies and F. Vierling, *Transition Met. Chem.*, 1999, **24**, 135–140.
50 H. F. Klein and H. H. Karsch, *Inorg. Chem.*, 1975, **14**, 473–477.
51 E. Bill, http://ewww.mpi-muelheim.mpg.de/bac/logins/bill/julX_en.php